Quasi-Direct Optical Transitions in Silicon Nanocrystals with Intensity Exceeding the Bulk

Benjamin G. Lee,[*,†] Jun-Wei Luo,[*,‡,§] Nathan R. Neale,[†] Matthew C. Beard,[†] Daniel Hiller,[∥] Margit Zacharias,[∥] Paul Stradins,[†] and Alex Zunger[⊥]

[†]National Renewable Energy Laboratory, Golden, Colorado 80401, United States

[‡]State Key Laboratory of Superlattices and Microstructures, Institute of Semiconductors, Chinese Academy of Sciences, Beijing 100083, China

[§]Synergetic Innovation Center of Quantum Information and Quantum Physics, University of Science and Technology of China, Hefei, Anhui 230026, China

[∥]Laboratory of Nanotechnology, IMTEK, Albert Ludwigs University, Freiburg 79110, Germany

[⊥]Renewable and Sustainable Energy Institute, University of Colorado, Boulder, Colorado 80309, United States

Ⓢ *Supporting Information*

ABSTRACT: Comparison of the measured absolute absorption cross section on a per Si atom basis of plasma-synthesized Si nanocrystals (NCs) with the absorption of bulk crystalline Si shows that while near the band edge the NC absorption is weaker than the bulk, yet above ~2.2 eV the NC absorbs up to 5 times more than the bulk. Using atomistic screened pseudopotential calculations we show that this enhancement arises from interface-induced scattering that enhances the quasi-direct, zero-phonon transitions by mixing direct Γ-like wave function character into the indirect X-like conduction band states, as well as from space confinement that broadens the distribution of wave functions in k-space. The absorption enhancement factor increases exponentially with decreasing NC size and is correlated with the exponentially increasing direct Γ-like wave function character mixed into the NC conduction states. This observation and its theoretical understanding could lead to engineering of Si and other indirect band gap NC materials for optical and optoelectronic applications.

KEYWORDS: Silicon nanocrystals, quantum dots, optical absorption, absorption cross section, atomistic screened pseudopotential
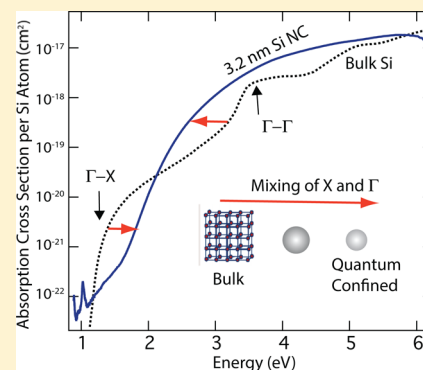
Silicon is ubiquitous in modern technology, being the dominant semiconductor material for the microelectronics and photovoltaic industries. However, its poor optical properties resulting from the indirect nature of its lowest energy optical transition have always hindered its use in photonic and optoelectronic applications. In bulk crystalline Si (c-Si) the conduction band minimum (CBM) occurs at the six equivalent Δ-valleys, located in the Brillouin zone along the [100] directions about 85% from the Γ-point out toward the X-point zone boundary, whereas the valence band maximum (VBM) occurs at the Γ-point. Thus, the fundamental band gap transition is momentum forbidden (indirect) so the zero-phonon transitions are dipole forbidden. A key challenge in silicon-based photonics is to control the intrinsic material properties to yield stronger optical transitions at the bandgap.[1] Indeed, the observation of bright photoluminescence (PL) first from highly porous Si[2−4] and then from Si nanocrystals (NCs)[2] launched an explosion of research aimed at understanding how the emission and absorption can be enhanced to the benefit of silicon-based photonics.[5−10]

In the current paper we focus on a concerted theoretical and experimental effort to understand and articulate the design principles that enhance interband transitions in Si NCs. We first clarify the (often confusing) roles of *momenta* ("band folding") versus the role of *state mixing* in the creation of strong absorption in NCs relative to the bulk solid, identifying the factors that need to be controlled to achieve such a change in absorption. We next measured the *absolute absorption cross section on a per Si atom basis* of plasma-synthesized and ligand-passivated Si NCs, comparing the results with the absorption of bulk c-Si, scaled with the local field factor correction for small particles. While the absorption of Si NCs has been measured previously,[11−14] ours is the first study to precisely determine the absorption on a *per Si atom basis* and compare with bulk c-Si. We demonstrate that above an energy of ~2.2 eV the NC absorbs up to 5 times stronger than the bulk.

Underlying Physics of Zero Phonon Absorption Strength in NCs Made of Indirect Band Gap Solids. The literature on absorption in Si nanostructures[11,12,15,16] lists many possible factors controlling the conversion of momen-

tum-forbidden to momentum allowed transitions as quasi-direct states, quantum confinement,[17] surface imperfections, and strain,[18] to name a few. We thus start by discussing the broader context of the underlying science that may lead to finite zero phonon transition intensity in NCs made of indirect gap solids.

As is well-known, each electronic state in translationally periodic crystalline solids can be classified by a single band $\{\phi_{n,\mathbf{k}}(\mathbf{r}) = u_{n,\mathbf{k}}(\mathbf{r})e^{i\mathbf{k}\cdot\mathbf{r}}\}$, belonging to a distinct wavevector k and band index n. Not surprisingly, the interband transitions between the valence and conduction bands are nonzero only if the wavevectors of the initial and final states are equal (momentum allowed direct transitions) in which case the intensity of the transition depends on the remaining factor, being the *orbital character* of the initial and final state with momentum (p) transition probability $P_{n_v,n_c} = <u_{n_v,\mathbf{k}}(\mathbf{r})|\hat{e}\cdot\mathbf{p}|u_{n_c,\mathbf{k}}(\mathbf{r})>$, reflecting the possibility of orbitally allowed vs orbitally forbidden transitions, associated with the point group selection rules. In contrast with such a relatively simple situation characterizing translationally periodic crystals, when translational periodicity is partially or fully removed, as is the case in nanostructures[19] or random bulk alloys,[20] then quantum mixing between the bulk Bloch states is allowed, and each nanostructure electronic state $\psi_{i,\mathbf{K}}(\mathbf{r})$ is a *superposition* of the bulk Bloch functions of the underlying perfect crystals

$$\psi_{i,\mathbf{K}}(\mathbf{r}) = \frac{1}{\sqrt{N}}\sum_{n}^{\infty}\sum_{\mathbf{k}}^{N_k} c_{i,n,\mathbf{K}}(\mathbf{k})u_{n,\mathbf{k}}(\mathbf{r})e^{i(\mathbf{k}+\mathbf{K})\cdot\mathbf{r}}$$

$$= \frac{1}{\sqrt{N}}\sum_{n}^{\infty}\sum_{\mathbf{k}}^{N_k} c_{i,n,\mathbf{K}}(\mathbf{k})\phi_{n,\mathbf{k}}(\mathbf{r})e^{i\mathbf{K}\cdot\mathbf{r}} \quad (1)$$

belonging to a *range* of wavevectors $\mathbf{k}$ and band indices n. Note that $\mathbf{K}$ is a wavevector in the mini Brillouin zone of the superstructure, which is finite only for superstructures remaining partially translational periodic, such as 2D quantum wells and 1D nanowires, otherwise $\mathbf{K} \equiv 0$ and the symbol is then omitted—for example in 0D NCs. In this case the interband transition probability includes contributions from different wavevectors $\mathbf{k}$ and different band components n of the underlying crystals:

$$\overline{P}_{v,c} = <\psi_{v,\mathbf{K}_v}|\hat{e}\cdot\mathbf{p}|\psi_{c,\mathbf{K}_c}>$$

$$= \frac{1}{N}\sum_{n_v}^{\infty}\sum_{n_c}^{\infty}\sum_{\mathbf{k}_v}^{N_k}\sum_{\mathbf{k}_c}^{N_k} c_{v,n_v,\mathbf{K}_v}^*(\mathbf{k}_v)c_{c,n_c,\mathbf{K}_c}(\mathbf{k}_c)$$

$$<\phi_{n_v,\mathbf{k}_v}|\hat{e}\cdot\mathbf{p}|\psi_{n_c,\mathbf{k}_c}>\delta_{\mathbf{K}_v\mathbf{K}_c}$$

$$= \frac{1}{N}\sum_{n_v}^{\infty}\sum_{n_c}^{\infty}\sum_{\mathbf{k}_v}^{N_k}\sum_{\mathbf{k}_c}^{N_k} c_{v,n_v,\mathbf{K}_v}^*(\mathbf{k}_v)c_{c,n_c,\mathbf{K}_c}(\mathbf{k}_c)$$

$$P_{n_v,n_c}\delta_{\mathbf{k}_v\mathbf{k}_c}\delta_{\mathbf{K}_v\mathbf{K}_c} \quad (2)$$

Here, $P_{n_v,n_c} = <u_{n_v,\mathbf{k}}(\mathbf{r})|\hat{e}\cdot\mathbf{p}|u_{n_c,\mathbf{k}}(\mathbf{r})>$ is the dipole matrix of *bulk* Si Bloch functions. It is well-established that the bulk Si crystal with its underlying tetrahedral point group symmetry has a *momentum* indirect bandgap transition (VBM at Γ-point and CBM at Δ-point), which is forbidden because the one and only nonzero expansion coefficient of the VBM is at Γ-point but of the CBM is at Δ-point. Together with the momentum conservation rule $\delta_{k_v k_c}$, this leads to $\overline{P}_{v,c} = 0$. To obtain finite

transition intensity one could either focus on restoring momentum conservation by coupling the right phonon to break the condition of $\delta_{k_v k_c}$ in eq 2 (a second order *phonon assisted* process which is generally weak and temperature-dependent[16]), or design sufficient deviations from translational symmetries that will cause the spread of the wave functions in k-space (multiple nonzero expansion coefficients) leading to finite zero-phonon transitions.[1] Here we are interested in the second avenue of designing an intense zero-phonon transition.

Accomplishing an intense zero-phonon transition from indirect band gap building blocks requires two different perturbations: first, placing both the nanostructure CBM and VBM at some K-point, say $\mathbf{K} = 0$, in the mini Brillouin zone; and second, placing sufficient Γ-component of the bulk Bloch functions possessed by the VBM in the final state (CBM) leading to the overlap in bulk Brillouin zone. The first step is essentially *geometrical* and can be achieved rather trivially by "band folding", leading to quasi-direct transitions. That this step is trivial and insufficient can be immediately recognized[1] by the *gedanken experiment* indicating that the creation of an artificial 2 × 2 × 2 unit cell of crystalline bulk Si would naturally fold the X-point of the bulk primary cell's FCC Brillouin zone onto the $\overline{\Gamma}$-point of the super cell mini Brillouin zone, leading formally to a direct system (VBM and CBM at same wavevector $\mathbf{K}$). However, the zero-phonon transition probability of eq 2 would remain exactly zero since quantum mixing between bulk Bloch functions is forbidden and the condition $\delta_{k_v k_c}$ is not broken, as the physical system of bulk crystalline Si has not been changed by the artificial construct of creating a larger unit cell of the same bulk Si crystal. Although the fact that such pseudo direct folded-in states have zero contribution to absorption in the absence of additional effects has been noted,[16] there has been considerable ongoing confusion in the literature.[21,22]

To achieve real transition intensity one needs to follow up the first step by the second step of creation of sufficient Γ-components of bulk Bloch functions possessed by the VBM in the X-like final state CBM. This might be done via a variety of chemical and structural perturbations that lead to orbital coupling relative to those of bulk Si. In terms of the formality of eq 2 this would be indicated by the creation of an overlap of nonzero coefficients $c_{i,n}(\mathbf{k})$ between the CBM and VBM for Si NCs. Such perturbations may include quantum confinement (kinetic energy enhancement via reduction in volume),[16] creation of interfaces or surfaces,[1] chemical passivation by ligands,[23] alloying, and strain,[23] deviations from the ideal tetrahedral T_d site symmetry, leading to interband and intervalley mixing.[1,24,25] We will refer to all such perturbations as "knobs" that lead to "*Bloch function coupling*" (BFC), making the wave function of eq 1 have a number of nonvanishing expanding coefficients (as opposed to only one nonzero coefficient), thus opening the door for the creation of sufficiently strong oscillator strength in eq 2. A recent example of the design of effective BFC in Si/Ge nanostructures is given by the identification of a "magic sequence" of Si and Ge monolayers in 2D superlattices, e.g., α-sequence $SiGe_2Si_2Ge_2SiGe_{12}$[1] and 1D core–multishell Si–Ge nanowires[24] where controlled reduction in orbital symmetry led to rather strong predicted absorption intensity. Here we enquire about the potential of such effects in 0D NCs. In numerous previous attempts to induce strong interband transitions in Si NCs, various chemical or structural perturbations were applied relative to bulk Si, and the ensuing absorption was

measured.[2−10,12,13,23,26] However, a direct link was rarely established between these structural and chemical knobs and the degree of BFC created. Here we offer a simple computational tool that establishes such a link and in principle offers the design of effective BFC-inducing knobs.

Theoretical Methodology Used To Establish the Direct Transition. The idea is to compute in the first step rather precisely the electronic structure of the NC, treating it as a large molecule (rather than drawing its properties from a reference effective mass description). We do so by explicitly incorporating in the relevant Schrödinger equation

$$\left(-\frac{\hbar^2}{2m}\nabla^2 + V(\mathbf{r}) \right)\psi_i(\mathbf{r}) = \epsilon_i\psi_i(\mathbf{r}) \quad (3)$$

with the crystal potential of the NC plus its matrix, both described as a superposition of atomic screened potentials v_α of atom type α at each atomic site $R_{\alpha,n}$ within the lattice site n: $V(\mathbf{r}) = \Sigma_{\alpha,n}v_\alpha(\mathbf{r} - \mathbf{R}_{\alpha,n})$.[27] This superposition construct naturally includes (with atomic resolution) the positions of all atoms in the NC as well as the explicit surface ligands of interfaces. These define the various engineering knobs that may control the BFC, including volume quantum confinement, deviations from ideal T_d symmetry, surface, and interface effects, etc. This Schrödinger equation is solved numerically (in a plane wave basis set) providing the wave functions used in eq 2 to describe the interband transition intensity. In the second step, and for the purpose of analysis only, we expand the numerically precise NC wave functions by a set of Bloch states of underlying perfect Si crystal, as in eq 1. This gives us the spectral function telling if the specific engineering degrees of freedom used create sufficient Γ character to produce strong absorption. It is straightforward from eq 1 that if we sum over the bands n at a given first Brillouin zone wavevector $\mathbf{k}$, we obtain the "majority representation" decomposition of the QD state i as[20]

$$p_i(\mathbf{k}) = \sum_n |<\psi_i(\mathbf{r})|u_{n,\mathbf{k}}e^{i\mathbf{k}\cdot\mathbf{r}}>|^2 \quad (4)$$

This quantity describes the amplitude of the bulk Bloch functions at any wavevector as it mixes into the quantum state (VBM, CBM, etc.) i and will be shown below in Figure 4. It thus supplies a direct link between structural or chemical engineering knobs (specified in the NC potential $V(\mathbf{r})$) and the ensuing state mixing accomplished. An auxiliary quantity useful for analysis is the weight functions ω_i^Γ, ω_i^X, and ω_i^L, which are defined by summing $p_i(\mathbf{k})$ over the k points contained in a spherical region around Γ, L, and X, respectively, as[19]

$$\omega_i^{\Gamma(X,L)} = \sum_{\mathbf{k}\in\Omega_{\Gamma(X,L)}} p_i(\mathbf{k}) \quad (5)$$

the spheres Ω_Γ, Ω_X, and Ω_L in the fcc Brillouin zone have the same radius. Figure 5a shows the Γ-component (ω_i^Γ) of each individual QD conduction band states.

Finally, we compute quantitatively the absorption of the NC and thereby numerically substantiate the insights derived from the analytical tool of Γ character. The no-phonon optical absorption spectrum $\alpha(\hbar\omega)$ in single-particle basis is calculated, given the dipole transition matrix $\overline{P}_{vc} = <v|\hat{e}\cdot\mathbf{p}|c>$, according to the Fermi golden rule:

$$\alpha(\hbar\omega) = \left(\frac{2\pi e}{m_0\omega}\right)^2 \sum_v \sum_c |\overline{P}_{vc}|^2 \exp\left[-\left(\frac{\hbar\omega - E_{vc}}{\lambda}\right)^2\right] \quad (6)$$

Here $E_{vc} = \epsilon_c - \epsilon_v$ is the transition energy from hole state v to electron state c, m_0 is the free-electron mass, and e is the free-electron charge, and λ represents the spectral line broadening. It gives the absorption in single-particle limit (e.g., no Coulomb and exchange interactions and no electron−electron correlation). In our previous work[25] we used the configuration interaction method to treat the many-body electron−hole interactions for the PL spectrum of Si NCs, finding that it redshifts the optical transitions by less than 0.1 eV and the excitonic fine structure by less than 1 meV. Therefore, we neglect the electron−hole Coulomb interaction in our current work, as we are interested in a large energy window (∼3 eV).

Overall, our three-step protocol provides both intuitive as well as quantitative prediction of the origin of absorption in Si NCs.

Experimental Determination of Si NC Optical Properties. *Synthesis.* We synthesized four samples of Si NCs with controlled sizes by silane decomposition in a radiofrequency-enhanced nonthermal plasma.[28] NCs are created in the plasma through electron impact dissociation of SiH_4 and subsequent clustering of the fragments. The NC surfaces are functionalized with dodecyl ligands via thermally induced reaction with 1-dodecene[29] rendering the NCs soluble in nonpolar solvents. Experimental details—including NC synthesis, ligand-capping, and measurement techniques—can be found in the Supporting Information, A: Synthesis.

Structural and Optical Characterization. Transmission electron microscopy (TEM) images of the dodecyl-capped Si NCs are shown in Figure 1. The ligands can be clearly seen on the edges of the NCs. Also, the visible lattice fringes are consistent with the diamond crystal structure of Si. The observed PL intensity of all samples is qualitatively strong;
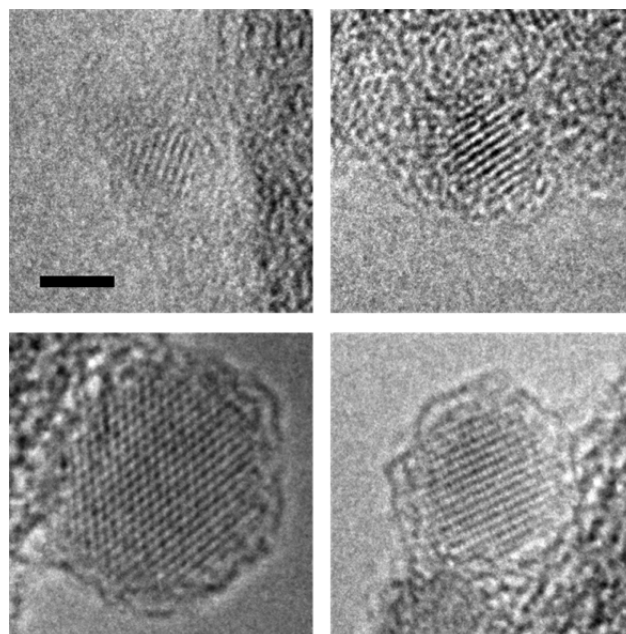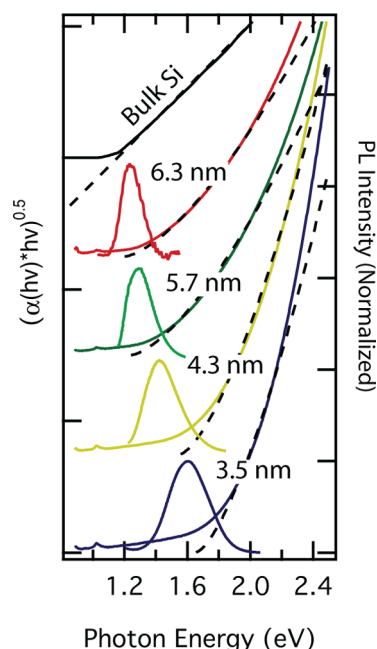

Figure 1. TEM images of plasma-synthesized Si NCs, with diameters of 3.2, 3.8, 6.3, and 7.8 nm (clockwise from top left). Scale bar is 2 nm, applies to all images. Lattice fringes are clearly visible in the NCs demonstrating that the NCs consist primarily of crystalline cores.

strong PL is associated with the crystalline phase, as opposed to amorphous nanoparticles that only emit weakly.[30] X-ray diffraction shown in the supplementary sections (Figure S1a) and Raman spectra (Figure S1b) measurements of the three larger diameter samples show clear evidence of crystalline Si. Though all samples contain crystalline cores, the smallest Si NCs feature more amorphous character at the NC surface than larger NCs—which exhibit an ordered, crystalline surface—based on decreasing PLQY values with decreasing NC size and FTIR analysis of the surface hydride region from our earlier study.[29]

Optical measurements including PL emission and absorption are performed on solutions of Si NCs in tetrachloroethylene (TCE) or hexane. To accurately determine the mass of Si NCs per volume of solvent, we use inductively coupled plasma optical emission spectroscopy (ICP-OES) to find the wt % of Si and C/H (hydrocarbon) in each sample; this allows us to subtract out the weight of the surrounding hydrocarbon ligand shells and accurately quantify the Si atom concentration for absorption measurements. For optical absorption experiments, samples are prepared at the highest concentration suitable for determining absorption close to the bandedge, where it is weak. Then, the solutions are successively diluted to measure the absorption at higher energies; we additionally prepare dilute solutions in hexane for energies >4 eV where TCE is not transparent. The measured transmission is scaled by the transmission of a control sample containing only the solvent, to account for reflection and other losses.

The PL emission and absorption near the band edge are plotted in Figure 2 (the data are vertically offset for clarity). The PL peak energies for the four samples are 1.59, 1.48, 1.29, and 1.24 eV. The absorption near the onset is plotted on a

Tauc scale $(\sigma \cdot h\nu)^{0.5}$ typically used to determine E_g and the nature of the optical transitions for disordered semiconductor thin films.[31] However, the data do not follow the linear dependence observed for bulk Si (Figure 2, black line) and expected for an indirect semiconductor, but rather exhibits a $(h\nu - E_0)^{1.5}$ dependence (Figure 2, dashed curves). This dependence and the increasing slope of the absorption with decreasing NC diameter is consistent with a transition from indirect to quasi-direct transitions. But it is not conclusive since the convolution from the NC size distribution[15] or subgap states[18] could also be responsible for the observed near band-edge behavior. Instead of this ensemble-average measurement, single-dot spectroscopy will be needed to fully resolve the issue.

We estimate the size of the NCs, in order to label the different samples and for ease of comparison with theoretical calculations. However, it is difficult to use direct measurements such as TEM or light-scattering to find the diameter and size distribution of ligand-capped NCs.[32,33] Therefore, we choose to infer the NC diameter from the quantum-confined band gap E_g^{NC}. For E_g^{NC} we use the PL peak energy, neglecting any potential Stokes shift. Then, from the atomistic pseudopotential calculation results of excitonic band gap as a function of NC diameter d for Si NCs embedded in oxide matrix:[25] $E_g = 1.1 + 2.5/d^{1.4}$ and experimentally measured PL peak energy, we estimate d and size distribution of each of the samples and find $d = 3.2$ (0.6), 3.8 (1), 6.3 (1), and 7.8 (2) nm, respectively. The value in parentheses represents the polydispersity of the samples (1σ deviation in the diameter). The PL fwhm (used to estimate the polydispersity) ranges from 0.16 to 0.3 eV, which is comparable to previously published results from plasma-synthesized NCs[28,30] and also from size-selected Si NCs embedded in SiO$_2$ deposited by the superlattice approach.[34]

Processing the Absorption Data to Extract Absolute Per Atom Absorption. We determine experimentally the optical absorption strength of Si NCs. To facilitate direct comparison between NCs having different sizes and also with bulk Si, we quantify the absorption cross-section σ_{Si}^{NC}, on a per Si atom basis. Using a per Si atom basis instead of a per NC one leads to a more accurate portrayal, due to the well-known difficulty of precisely determining NC sizes and also their size distribution. Moreover, it facilitates the important comparison with bulk Si, which allows us to distinguish the effects of quantum confinement. However, the absorption cross-section σ_{Si} of bulk Si must be scaled according to a *local field factor correction.* The local field factor correction accounts for the classical effect of reduced effective absorption, when a small particle (compared with the wavelength of light) is located within a lower refractive index dielectric.[35,36] This corresponds to our actual experimental situation, where the Si NCs are dilutely dispersed in TCE (refractive index $n = 1.47$) solution for the measurements. With the scaling, we can take into account this classical effect, and focus on the absorption differences with bulk Si that arise from quantum confinement.

We outline a derivation of the frequency-dependent local field factor correction, following ref 35. Consider a small dielectric sphere, embedded in a medium with different dielectric function $\varepsilon_0(\omega)$. At any given moment in time, the particle sees a constant electric field, and is polarized. Also for $\varepsilon_0(\omega) < \varepsilon(\omega)$, the electric field inside the sphere is reduced:

Figure 2. PL (peaks) and absorption (curves) near the band edge of plasma-synthesized Si NCs, with diameters of 3.2 (0.6), 3.8 (1), 6.3 (1), and 7.8 (2) nm. Data are vertically offset for clarity. Dashed curves associated with the NCs highlight the $(h\nu - E_0)^{1.5}$ dependence of the band edge absorption. The one-standard deviation in the size distribution is noted in parentheses and corresponds to ~20% size distributions.

$$P = \frac{3\varepsilon_0(\varepsilon - \varepsilon_0)}{\varepsilon + 2\varepsilon_0}E_0 \qquad (7)$$

$$E = \frac{3\varepsilon_0}{\varepsilon + 2\varepsilon_0} E_0 \tag{8}$$

Thus, the absorption of the sphere is also reduced:

$$\sigma_{Si}^{NC} = -<D \cdot \frac{dE}{dt}> \sim \frac{n_{bulk}}{n_0} \left(\frac{3\varepsilon_0}{\varepsilon_{bulk} + 2\varepsilon_0} \right)^2 \sigma_{Si}^{bulk} \tag{9}$$

Note that the derived absorption is proportional to the volume of the nanoparticle; thus when normalized to a per Si atom basis, the same correction factor applies for all particle radii.

Moreover, the per Si atom normalization is more accurate than normalizing to average NC size, since there is variability in the NC diameter within each sample, in addition to the inherent uncertainty in the size determination. The per Si atom normalized optical absorption of NCs compared with (local bulk field factor corrected) bulk c-Si is shown in Figure 3.
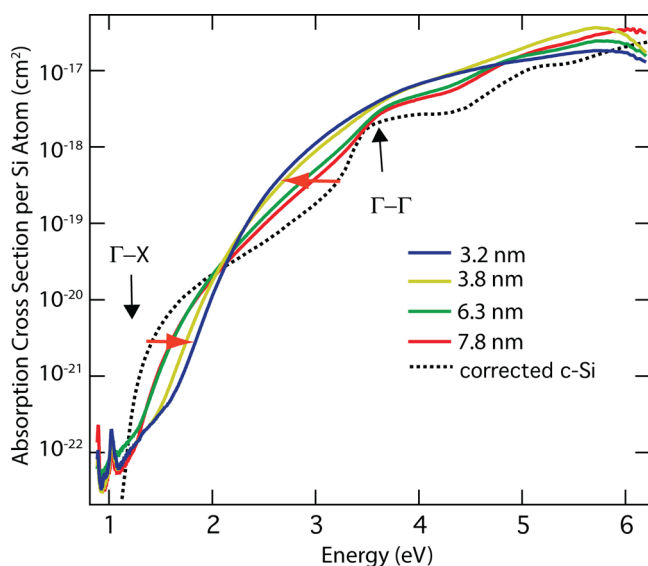

Figure 3. Comparison of σ_{Si}^{NC} on a per Si atom basis of plasma-synthesized Si NCs with the absorption of bulk c-Si scaled to account for the local field factor correction in small particles. The peak near 1 eV in the NC data arises from a solvent mode. The NC data also show a clear sub-bandgap absorption.

Comparison of NC and Bulk Absorption. We find two regimes in the optical absorption of Si NCs (Figure 3). In the low-energy region, we find that σ_{Si}^{NC} is reduced for energies starting at the bulk band gap of Si (1.1 eV) to ~2.2 eV (Figure 3). Here, there is a clear trend of smaller NCs having blue-shifted absorption onset and thus lower absorption intensity than bulk Si, as expected from quantum confinement of their bandgap energies. At >2.2 eV, there is enhanced absorption up to at least the direct band gap of bulk Si (Γ−Γ point at 3.4 eV, Figure 3); in this region, σ_{Si}^{NC} is above that of (local field factor corrected) bulk c-Si. Moreover, the magnitude of the absorption enhancement in this region increases with decreasing NC size. This is a noteworthy experimental result, one which we have focused our attention on explaining.

These results are repeatable when care is taken to quantify the absolute strength of the optical absorption. We have additionally measured σ_{Si}^{NC} of 5 nm diameter Si NCs embedded in SiO$_2$ and prepared according to ref 34. Nearly identical results were seen (see Supplementary Info, Figure S2). The

distinct surface chemistries of NCs embedded in an oxide matrix versus hydrocarbon-capped species would lead to drastically different optical properties if they were associated with surface states from interfaces or ligands. This observation points to quantum confinement as the cause of the enhanced absorption. Further experimental support comes from the quantitative absorption cross sections found by ref 13 for plasma-synthesized Si NCs from 5.1 to 10 nm, which also hinted at an enhancement above the classical prediction. The observed absorption enhancement is consistent with a conservation of total oscillator strength where quantum confinement shifts the oscillator strength from lower energy transitions to higher energy transitions. In the following theoretical analysis, we endeavor to understand and explain the origin of this effect.

Discussion of the Origins of Enhanced Zero Phonon Absorption. Figure 4 shows the k-space distribution eq 4 of the CBM (upper row, electrons) and the VBM (lower row, holes) for two Si NCs (sizes D = 8 nm in Figure 4a and 1.4 nm in Figure 4b). In the Si NCs as shown in Figures 4a and 4b, the
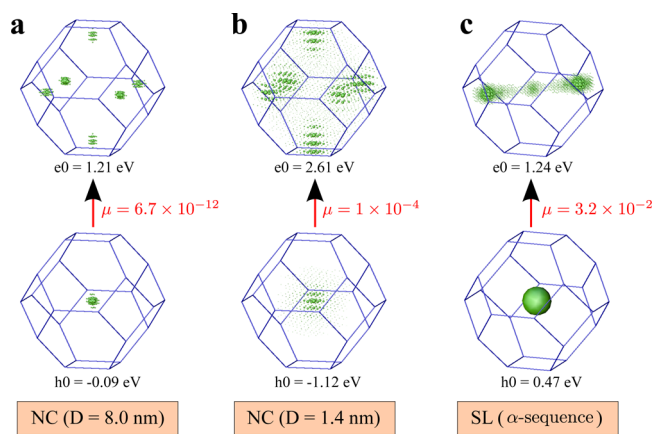
Figure 4. Degree of mixing (eq 4) of bulk Bloch functions at various wavevectors in the FCC Brillouin zone within the NC wave functions of the CBM and VBM: (a) Si NC with size D = 8 nm; (b) NC with size D = 1.4 nm; (c) α-sequence (SiGe$_2$Si$_2$Ge$_2$SiGe$_{12}$) Si/Ge superlattice (SL). The energies of CBM and VBM relative to the bulk Si VBM are given beneath the corresponding wave function plots, and the dipole matrix element μ is also given.

VBM wavevector character is centered around the Γ-point and exponentially decays away from there, while the CBM wavevector character is most centered at the Δ-point and exponentially decays away from there. The corresponding eigenvalues relative to bulk Si VBM are given beneath the plots of wave function. We see that as the NC size is reduced (so the confinement energy increases) the extent of spread in k-space of both CBM and VBM increase. In addition to the 0D Si NCs, we also show in Figure 4c the k-space distribution of CBM and VBM for a Si/Ge 2D superlattice (SL) that was recently inverse designed to have strong optical emission.[1] In comparison to the two Si NCs, the SL possesses a striking feature that the CBM has a local maximum at the Γ-point in addition to its global maxima at the Δ-point and spreads in k-space along the [001] direction (i.e., the SL growth direction).

Figure 5 shows the Γ-component ω_i^Γ of each calculated NC conduction band electronic state for NCs of 3 and 4 nm, by projecting onto the bulk Si Bloch functions (eq 5). The energy scale is measured from the top of the valence band of bulk Si.
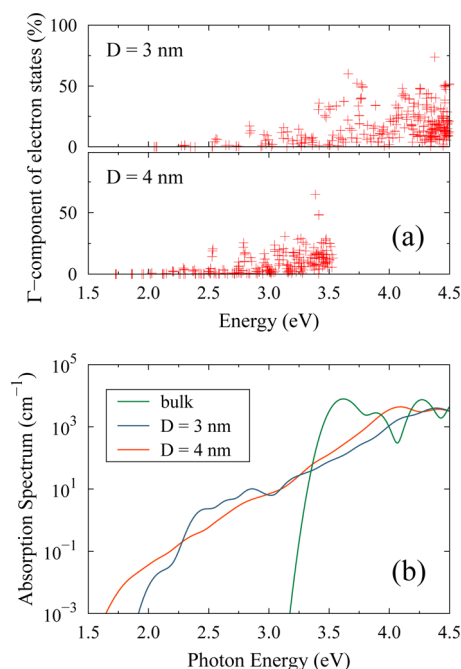
Figure 5. (a) Fraction of Γ-component of bulk Bloch functions in each conduction band electronic state, for Si NCs with diameters 3 and 4 nm. Each individual red "+" corresponds to a single electronic state. The energy scale is measured from the top of the NC valence band. For D = 4 nm, the electron states are calculated up to ~3.5 eV. (b) Calculated zero-phonon absorption spectrum for Si NCs with diameters of 3 and 4 nm. The absorption calculation excludes all phonon-assisted processes, showing only quasi-direct transitions.

Significantly, even for larger NCs (e.g., 4 nm size) we see appreciable Γ-component in the conduction band states. Specifically, the presence of Γ-component exists in numerous states below 3.4 eV (Γ–Γ transition in bulk Si). Thus, there is increased likelihood of quasi-direct optical transitions. This quasi-direct character can be seen in the calculated zero-phonon optical absorption (Figure 5b) of 3 and 4 nm diameter NCs; this calculation excludes all phonon-assisted processes, showing only quasi-direct transitions. It is clear from these calculations that zero-phonon transitions are allowed at much lower energies for quantum-confined NCs than in bulk Si.

The momentum conservation law of optical transition, which forces the band gap transition of bulk Si to be strictly forbidden, is partially relaxed in Si NCs leading to the enhancement of optical transition in Si NCs. This relaxation was attributed earlier to the Heisenberg uncertainty principle $\Delta r \cdot \Delta k > 1/2$, where r is the NC radius and k is the wavevector of QD electrons or holes.[37] This is a result of space reduction in a NC leading to a spread in momentum, a spread that induces the possibility of the overlap of electron and hole wave function in k-space and thus allows the optical transitions (eq 2). This mechanism alone would predict that the k-space wave function of the CBM (VBM) in Si NCs should be mostly centered at the Δ-point (Γ-point) and exponentially decay away from there. The extent of the spread is inversely proportional to the NC size. Along with the k-space spread of wave functions, the space confinement also increases the energy of quantized states as the NC size is reduced (to the power of 1–2).[25] Thus, the quantum confinement should result in a power law scale of light emission and confinement energy on NC size. These features of space quantum confinement effects are in excellent

agreement with that of our atomistic pseudopotential calculated results for Si NCs, as shown in Figure 5a and b.

This agreement demonstrates that the space confinement dominates the relaxation of momentum conservation for Si NCs. However, the space confinement effect is not the only cause of the spread of the wave function. We propose a mechanism, where the spread of electron and hole wave functions arises from scattering at the interface causing Γ–X intervalley coupling, giving an admixture of Γ-character to X-valley dominated conduction band states, and enabling an increase in quasi-direct transitions. This line of reasoning is bolstered by the results of our recent work[1] to reveal specific Si/Ge superlattices (e.g., α-sequence $SiGe_2Si_2Ge_2SiGe_{12}$ superlattice) that have optically allowed, direct gap transitions resulting from an enhanced Γ–X coupling. There we found that the oscillator strength of band-edge transitions can be changed by orders of magnitude, even while the band gap E_g was nearly constant, just by varying the Si and Ge layer sequences. The enhanced zero-phonon transition comes from increased Γ–X coupling at the conduction band edge[1] as shown in Figure 4c where the CBM has a local maximum at the Brillouin zone center Γ-point with the global maximum at Δ-points. Therefore, the relaxation of momentum conservation rule observed in the specific Si/Ge superlattices is due to a new mechanism, which we propose be called interface scattering, and is distinct from the Heisenberg uncertainty principle.

This surface scattering mechanism is evidenced in the NC excited electron states. Figure 5a shows that some of the NC electron states located below 3.5 eV in energy have too large Γ-component of bulk Bloch functions to be explained by the Heisenberg uncertainty principle alone. This is since they are derived from the X-valley and their Γ-component is expected to be small when reckoning from the uncertainty principle. However, the surface scattering mechanism leads to Γ–X mixing with magnitude inversely proportional to the energy separation between X-like and Γ-like NC states. For X-like electron states with energies approaching the Γ-like states, their Γ-component might increase significantly. This explains why we can find electron states possessing around 50% Γ-component but lower lying (in energy) than the bulk Γ-valley. Bearing in mind this new mechanism, we could engineer the NC surface to significantly enhance the optical transition intensity.

We conclude that the relaxation of the momentum conservation rule in Si NCs are joint effects of both the Heisenberg uncertainty principle and interface scattering-induced Γ–X coupling. The mechanism of surface scattering-induced Γ-X coupling may provide a novel route to engineer NC surfaces (e.g., varying roughness, shape, or alloying)[26] to further enhance the radiative rate of Si NCs. For example, a Si NC core with a Si/Ge multiple shell may result in an engineered band structure that further enhances the strength of optical transition. Additional investigation may permit the design and engineering of quantum-confined materials with strongly enhanced absorption and emission properties by leveraging this new interface scattering mechanism.

Conclusions. In summary, we have investigated the relaxation of k-conservation that allows quasi-direct optical transitions for Si NCs. We find that this relaxation occurs since the NCs are not translationally invariant, due to their small finite size and the presence of the interfaces/surfaces. Thus, the energy states of the NCs will look like a spectral mixing of the (bulk) crystalline Si Brillouin zone. Quantitatively, our atomistic screened pseudopotential calculations indicate many

conduction band states of the NC core have a mix of X- and Γ-character. This appreciable Γ-component permits zero-phonon, quasi-direct optical transitions in the Si NCs, at energies between the quantum-confined band gap in NCs and the bulk c-Si direct band gap at 3.4 eV. This helps explain the experimentally observed enhanced absorption between ∼2.2 and 3.4 eV for quantum-confined Si NC samples.

■ ASSOCIATED CONTENT

Ⓢ Supporting Information

The Supporting Information is available free of charge on the ACS Publications website at DOI: 10.1021/acs.nano-lett.5b04256.

> Details of synthesis/preparation and measurements of Si nanocrystal samples, including both plasma-synthesized Si NCs and Si NCs in oxide matrix (PDF)

■ AUTHOR INFORMATION

Corresponding Authors
*E-mail: benjamin.lee@nrel.gov.
*E-mail: jwluo@semi.ac.cn.

Author Contributions

Both corresponding authors contributed equally to the paper.

Notes

The authors declare no competing financial interest.

■ ACKNOWLEDGMENTS

■ REFERENCES

(1) d'Avezac, M.; Luo, J.-W.; Chanier, T.; Zunger, A. *Phys. Rev. Lett.* **2012**, *108* (2), 027401.
(2) Furukawa, S.; Miyasato, T. *Phys. Rev. B: Condens. Matter Mater. Phys.* **1988**, *38* (8), 5726.
(3) Canham, L. T. *Appl. Phys. Lett.* **1990**, *57* (10), 1046–1048.
(4) Lehmann, V.; Gösele, U. *Appl. Phys. Lett.* **1991**, *58* (8), 856–858.
(5) Baehr-Jones, T.; Pinguet, T.; Guo-Qiang, P. L.; Danziger, S.; Prather, D.; Hochberg, M. *Nat. Photonics* **2012**, *6* (4), 206–208.
(6) Iyer, S. S.; Xie, Y.-H. *Science* **1993**, *260* (5104), 40–46.
(7) Asghari, M.; Krishnamoorthy, A. V. *Nat. Photonics* **2011**, *5* (5), 268–270.
(8) Ng, W. L.; Lourenco, M. A.; Gwilliam, R. M.; Ledain, S.; Shao, G.; Homewood, K. P. *Nature* **2001**, *410* (6825), 192–194.
(9) Green, M. A.; Zhao, J.; Wang, A.; Reece, P. J.; Gal, M. *Nature* **2001**, *412* (6849), 805–808.
(10) Hirschman, K. D.; Tsybeskov, L.; Duttagupta, S. P.; Fauchet, P. *Nature* **1996**, *384* (6607), 338–341.
(11) Meier, C.; Gondorf, A.; Lüttjohann, S.; Lorke, A.; Wiggers, H. *J. Appl. Phys.* **2007**, *101* (10), 103112.
(12) Holmes, J. D.; Ziegler, K. J.; Doty, R. C.; Pell, L. E.; Johnston, K. P.; Korgel, B. A. *J. Am. Chem. Soc.* **2001**, *123* (16), 3743–3748.
(13) Gresback, R.; Murakami, Y.; Ding, Y.; Yamada, R.; Okazaki, K.; Nozaki, T. *Langmuir* **2013**, *29* (6), 1802–1807.
(14) Mustafeez, W.; Majumdar, A.; Vučković, J.; Salleo, A. *J. Appl. Phys.* **2014**, *115* (10), 103515.
(15) Kovalev, D.; Diener, J.; Heckler, H.; Polisski, G.; Künzner, N.; Koch, F. *Phys. Rev. B: Condens. Matter Mater. Phys.* **2000**, *61* (7), 4485–4487.
(16) Hybertsen, M. S. *Phys. Rev. Lett.* **1994**, *72* (10), 1514.
(17) Delley, B.; Steigmeier, E. F. *Phys. Rev. B: Condens. Matter Mater. Phys.* **1993**, *47* (3), 1397–1400.
(18) Lee, B. G.; Hiller, D.; Luo, J.-W.; Semonin, O. E.; Beard, M. C.; Zacharias, M.; Stradins, P. *Adv. Funct. Mater.* **2012**, *22* (15), 3223–3232.
(19) Luo, J.-W.; Franceschetti, A.; Zunger, A. *Phys. Rev. B: Condens. Matter Mater. Phys.* **2008**, *78* (3), 035306.
(20) Wang, L.-W.; Bellaiche, L.; Wei, S.-H.; Zunger, A. *Phys. Rev. Lett.* **1998**, *80* (21), 4725.
(21) Zhao, X.; Wei, C. M.; Yang, L.; Chou, M. Y. *Phys. Rev. Lett.* **2004**, *92* (23), 236805.
(22) Li, D. X.; Feng, J. Y. *Appl. Phys. Lett.* **2008**, *92* (24), 243117.
(23) Dohnalová, K.; Gregorkiewicz, T.; Kůsová, K. *J. Phys.: Condens. Matter* **2014**, *26* (17), 173201.
(24) Zhang, L.; d'Avezac, M.; Luo, J.-W.; Zunger, A. *Nano Lett.* **2012**, *12* (2), 984–991.
(25) Luo, J.-W.; Stradins, P.; Zunger, A. *Energy Environ. Sci.* **2011**, *4* (7), 2546–2557.
(26) Dohnalová, K.; Poddubny, A. N.; Prokofiev, A. A.; de Boer, W. D.; Umesh, C. P.; Paulusse, J. M.; Zuilhof, H.; Gregorkiewicz, T. *Light: Sci. Appl.* **2013**, *2* (1), e47.
(27) Wang, L. W.; Zunger, A. *Phys. Rev. B: Condens. Matter Mater. Phys.* **1995**, *51* (24), 17398.
(28) Mangolini, L.; Thimsen, E.; Kortshagen, U. *Nano Lett.* **2005**, *5* (4), 655–659.
(29) Wheeler, L. M.; Anderson, N. C.; Palomaki, P. K. B.; Blackburn, J. L.; Johnson, J. C.; Neale, N. R. *Chem. Mater.* **2015**, *27*, 6869.
(30) Anthony, R.; Kortshagen, U. *Phys. Rev. B: Condens. Matter Mater. Phys.* **2009**, *80* (11), 115407.
(31) Pankove, J. I. *Optical processes in semiconductors*; Prentice-Hall, 1971.
(32) Hessel, C. M.; Reid, D.; Panthani, M. G.; Rasch, M. R.; Goodfellow, B. W.; Wei, J.; Fujii, H.; Akhavan, V.; Korgel, B. A. *Chem. Mater.* **2012**, *24* (2), 393–401.
(33) Wen, X.; Zhang, P.; Smith, T. A.; Anthony, R. J.; Kortshagen, U. R.; Yu, P.; Feng, Y.; Shrestha, S.; Coniber, G.; Huang, S. *Sci. Rep.* **2015**, *5*, 12469.
(34) Zacharias, M.; Heitmann, J.; Scholz, R.; Kahler, U.; Schmidt, M.; Bläsing, J. *Appl. Phys. Lett.* **2002**, *80* (4), 661.
(35) Landau, L. D.; Bell, J. S.; Kearsley, M. J.; Pitaevskii, L. P.; Lifshitz, E. M.; Sykes, J. B. *Electrodynamics of continuous media*; Elsevier, 1984; Vol. 8.
(36) Leatherdale, C. A.; Woo, W.-K.; Mikulec, F. V.; Bawendi, M. G. *J. Phys. Chem. B* **2002**, *106* (31), 7619–7622.
(37) Belyakov, V. A.; Burdov, V. A.; Lockwood, R.; Meldrum, A. *Advances in Optical Technologies* **2008**, *2008*, 1–32.